Int. J. Electrochem. Sci., 14 **(2019)** 4226 – 4239, doi: 10.20964/2019.05.10

International Journal of ELECTROCHEMICAL SCIENCE
www.electrochemsci.org

Corrosion behavior of Zn-TiO_2 and Zn-ZnO Electrodeposited Coatings in 3.5% NaCl solution

J. A. Cabral-Miramontes,[1] D. M. Bastidas,[2] M. A. Baltazar[3]., P. Zambrano-Robledo.,[1] J. M. Bastidas,[4] F. M. Almeraya-Calderón,[1] C. Gaona-Tiburcio[1]*

[1] Universidad Autónoma de Nuevo León, Facultad de Ingeniería Mecánica y Eléctrica, Centro de Investigación e Innovación en Ingeniería Aeronáutica (CIIIA), Av. Universidad s/n, Ciudad Universitaria, San Nicolás de los Garza, Nuevo León 66455, México
[2] National Center for Education and Research on Corrosion and Materials Performance, NCERCAMP-UA, Dept. Chemical and Bimolecular Engineering, The University of Akron, 302 E Buchtel Ave, Akron, OH 44325-3906, United States
[3] Universidad Veracruzana – Facultad de Ingeniería Civil-Xalapa, Circuito Gonzalo Aguirre Beltrán s/n, Zona Universitaria 91090, Xalapa, Veracruz, México
[4] Centro Nacional de Investigaciones Metalúrgicas (CENIM), CSIC, Av. Gregorio del Amo 8, 28040 Madrid, Spain
[*]E-mail: citlalli.gaonatib@uanl.edu.mx

Received: 11 September 2018 / *Accepted:* 11 November 2018 / *Published:* 10 April 2019

Electrodeposition is a widely used method to protect metallic materials from corrosion. Electrodeposited coatings provide the metal substrate with both cathodic protection and a barrier effect. The corrosion resistance achieved with this type of zinc-electroplating process in increased by adding nanometric materials to the electrolytic bath. In the present research, coatings were obtained by electrodeposition of pure zinc, Zn-TiO_2 and Zn-ZnO nanoparticles. The coatings were generated by immersion in a chloride acid bath applying a current density of 0.05 and 0.10 A/cm^2 for 1 min and adding 2 g/l of TiO_2 or ZnO nanoparticles. Corrosion behaviour was evaluated with potentiodynamic polarization curves and the electrochemical impedance spectroscopy (EIS) technique using a 3.5% NaCl test solution. After electrochemical testing, the coating surface morphology was analysed by scanning electron microscopy (SEM) and the atomic composition by energy dispersive X-ray spectroscopy (EDS). The electrodeposited coating thickness was measured using the ultrasound technique. The coating thickness was less than 2.5 μm and its corrosion resistance increased with the addition of nanoparticles.

Keywords: Electrodeposition, Zn-coatings, Corrosion, Nanoparticles, Composite Coatings,

1. INTRODUCTION

Current trends in electroplating are moving towards the production of surface coatings that are not only visually attractive but also functional structures. The electrodeposition of different solutions focuses on achieving a controlled and defined solid/electrolyte interface where these functional structures can be formed. The need to develop coatings with improved corrosion resistance to aggressive environments is also receiving growing interest as a result of the increasing demand for industrial components with a longer service life. Steel is one of the most widely employed materials in industry due to its low cost and recyclability, but its use is limited by its low corrosion resistance. Coatings have long been applied to protect steel from corrosion, and galvanized coatings (zinc coating, tropicalized, paints and organic coatings) are among the most used. Electrodeposition is one of the commonest methods for growing a deposited coating and the electrodeposition of zinc (applied on the surface of a steel substrate) is one of the most popular processes for protecting steel. The electrochemical deposition processes requires the presence of an anode, a cathode, an electrolytic solution containing ions of the material to be deposited on the substrate, and an external power source. Besides being cheap and very simple, the electrodeposition method usually produces materials or nanostructures that cannot be obtained by other deposition techniques [1].

Several studies have shown that particles electrochemically embedded in the coating confer the final electrodeposited coating with special properties that can respond to different industrial applications, such as wear resistance, self-lubrication and corrosion resistance [2−4]. Zinc coatings are widely used on steel substrates to control the corrosion process, and in this respect zinc alloy coatings present better corrosion resistance than pure zinc coatings. Compound coatings containing zinc and nanoparticles such as carbon nanotubes, TiO_2 nanoparticles, silica, silicon carbide, ceramic powders and Fe_2O_3, are becoming increasingly important thanks to their improved corrosion resistance properties [5−8]. The properties of composite zinc-nanoparticle coatings can be set to the desired level by adjusting the amount of nanoparticles in the coating and the electrochemical parameters of the manufacturing process [9,10].

Some studies have shown that electrochemically generated compound coatings of zinc with carbon nanotubes exhibited excellent corrosion resistance in aggressive media containing chlorides. Similar studies reported that nanocomposites with black carbon, Zn-TiO_2 and Zn-carbon nanoparticles afford improved corrosion protection to steel [11,12]. Zinc nanocomposite coatings are usually obtained by the electrodeposition method due to the fact that this a simple, low-temperature process with a high deposition rate and a low cost, in which the nanoparticles adhere well to the matrix of the material to be coated, with simultaneous reduction of the metal ions found at the electrode/solution interface [13−16].

The aim of this paper is to assess the corrosion behaviour of zinc nanocomposite coatings generated in an electrolytic bath containing zinc ions and nanoparticles of TiO_2 and ZnO. The electrochemical properties of the composite coatings have been studied by potentiodynamic polarization and electrochemical impedance spectroscopy techniques using a 3.5% NaCl test solution.

2. EXPERIMENTAL PROCEDURE

Pure zinc and composite coatings (TiO_2 and ZnO) were electrodeposited on a 1018 carbon steel substrate with the chemical composition: 0.18 wt.% C, 0.8 wt.% Mn, 0.04 wt.% P, 0.05 wt.% S, balance Fe, using an electrolytic bath solution. The chemical composition of the bath solution was: $ZnCl_2$ (90 g/l), KCl (100 g/l), $Na_3C_6H_5O_7 \cdot 2H_2O$ (10 g/l), EDTA-2Na (4 g/l), H_3BO_3 (35 g/l), and 2 g/l of TiO_2 or ZnO nanoparticles. The electrochemical cell used high purity zinc 99.99% as the anode, and 1018 carbon steel as the cathode. The anode was activated by immersion in a 10% HCl solution for 30 s and immediately after rinsed with distilled water. Fig. 1 shows the electroplating procedure. Experimental tests were performed at 25 ºC temperature, 1 min immersion time in the bath solution and pH 4. The electrodeposition process under galvanostatic conditions was carried out using a conventional DC power source, applying a current density of 0.05 A/cm^2 or 0.10 A/cm^2. The bath solution was stirred by air bubbling during the coating process. The cathode surface finish was obtained by mechanical polishing. The carbon steel plates were immersed in a 10% HCl solution for 1 min, and immediately after rinsed with distilled water, before final electroplating in the bath solution.

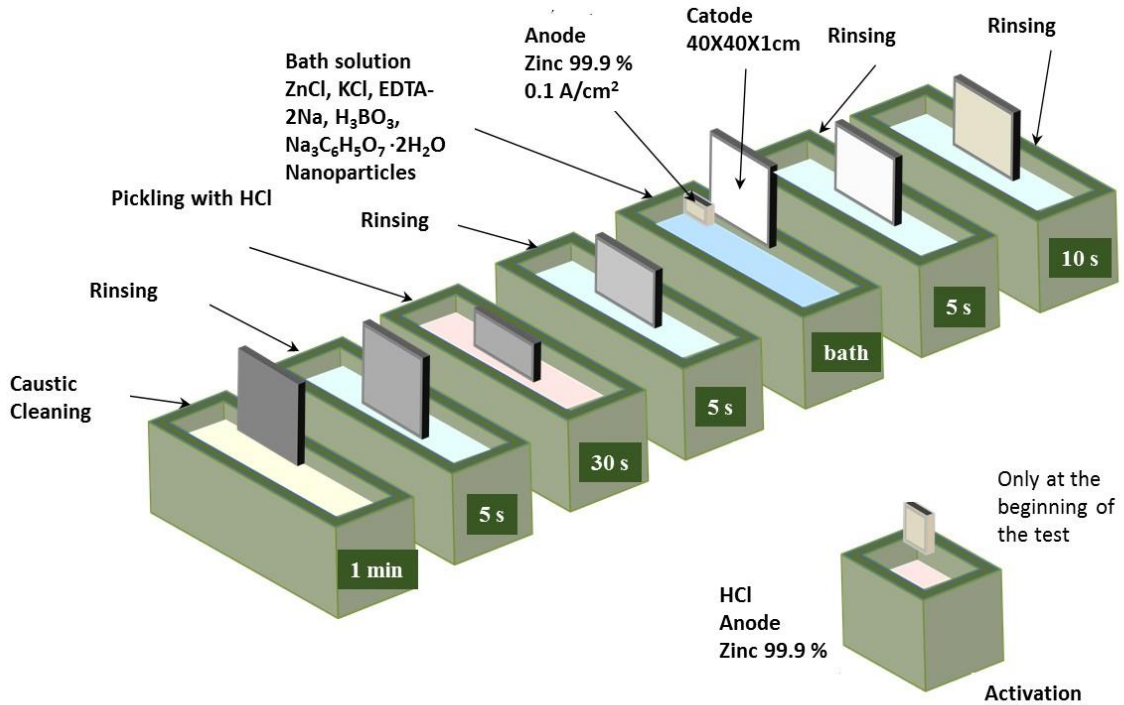

Figure 1. Electrogalvanizing process for producing nanoparticle composite coatings.

The ultrasound technique was used to measure the final thickness of the coatings. The surface morphology was analysed by scanning electron microscopy (SEM) and energy dispersive X-ray spectroscopy (EDS).

Corrosion experiments were performed by immersion of the coated specimens, with an exposed surface area of 1.0 cm^2, in a 3.5% NaCl solution, pH neutral at 25 ºC temperature.

A conventional 3-electrode cell configuration was used for electrochemical studies. The coated steel specimens with pure zinc, Zn-TiO_2 or Zn-ZnO were used as the working electrode. A saturated calomel electrode (SCE) and a platinum mesh were used as reference and counter electrode, respectively. Electrochemical measurements were carried out using a Gill-AC potentiostat/galvanostat/ZRA from ACM Instruments. Potentiodynamic polarization curves were recorded at a sweep rate of 60 mV/min, according to ASTM G5-11 standard [17]. A potential scan range was applied between −300 mV and +1500 mV vs. SCE. Electrochemical impedance spectroscopy (EIS) measurements were recorded at the corrosion potential (E_{corr}) over a frequency range from 10 kHz to 10 mHz, obtaining 10 points per decade and applying 10 mV r.m.s. amplitude according to ASTM G106-15 standard [18].

3. RESULTS AND DISCUSSION

3.1 Coating Thickness

The thickness of the pure zinc, Zn-TiO_2 and Zn-ZnO composite nanoparticle coatings is shown in Fig. 2. It can be seen that the pure zinc coating is thicker than composite coatings containing Zn-TiO_2 and Zn-ZnO nanoparticles (except for pure zinc using a 0.05 A/cm^2 current density and Zn-ZnO), probably due to the fact that the addition of nanoparticles causes a modification in crystal growth and increases the number of nucleation sites, thus reducing the grain size [7]. The growth of electrodeposited layers is a competition between nucleation and crystal growth, and as nanoparticles provide more nucleation sites, they therefore retard crystal growth.

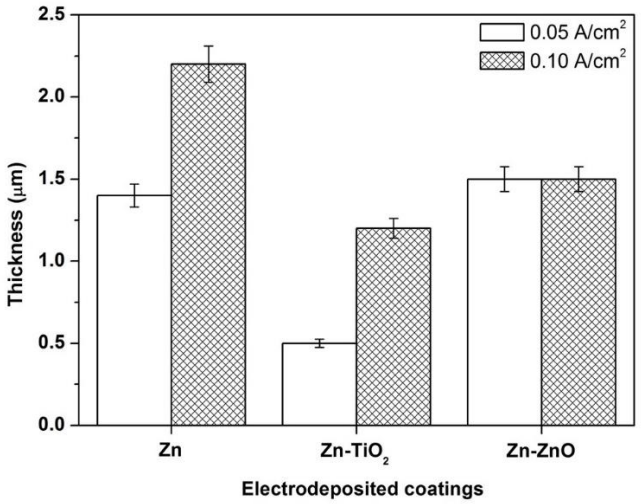

Figure 2. Electrodeposited pure zinc and zinc-nanoparticle (Zn-TiO_2 and Zn-ZnO) coating thickness.

3.2 Coating Surface Morphology

SEM micrographs showing the crystal microstructures of pure zinc, Zn-TiO_2 and Zn-ZnO nanocoatings are included in Figs. 3 and 4 using 0.05 and 0.10 A/cm^2 current density, respectively. Fig. 3(a) shows the microstructure of pure zinc with characteristic crystals, while Fig. 3(c) shows the Zn-TiO_2 composite coating microstructure including areas without any apparent coating and heterogeneous crystals that tend to form hexagonal platelets. Fig. 3(f) shows the Zn-ZnO composite coating microstructure, revealing a morphology with a non-uniform crystal grain distribution. The EDS spectra of Fig. 3(b,d,e,g,h) show the presence of Fe and Zn, with an inhomogeneous distribution of zinc in the electrodeposited coating.

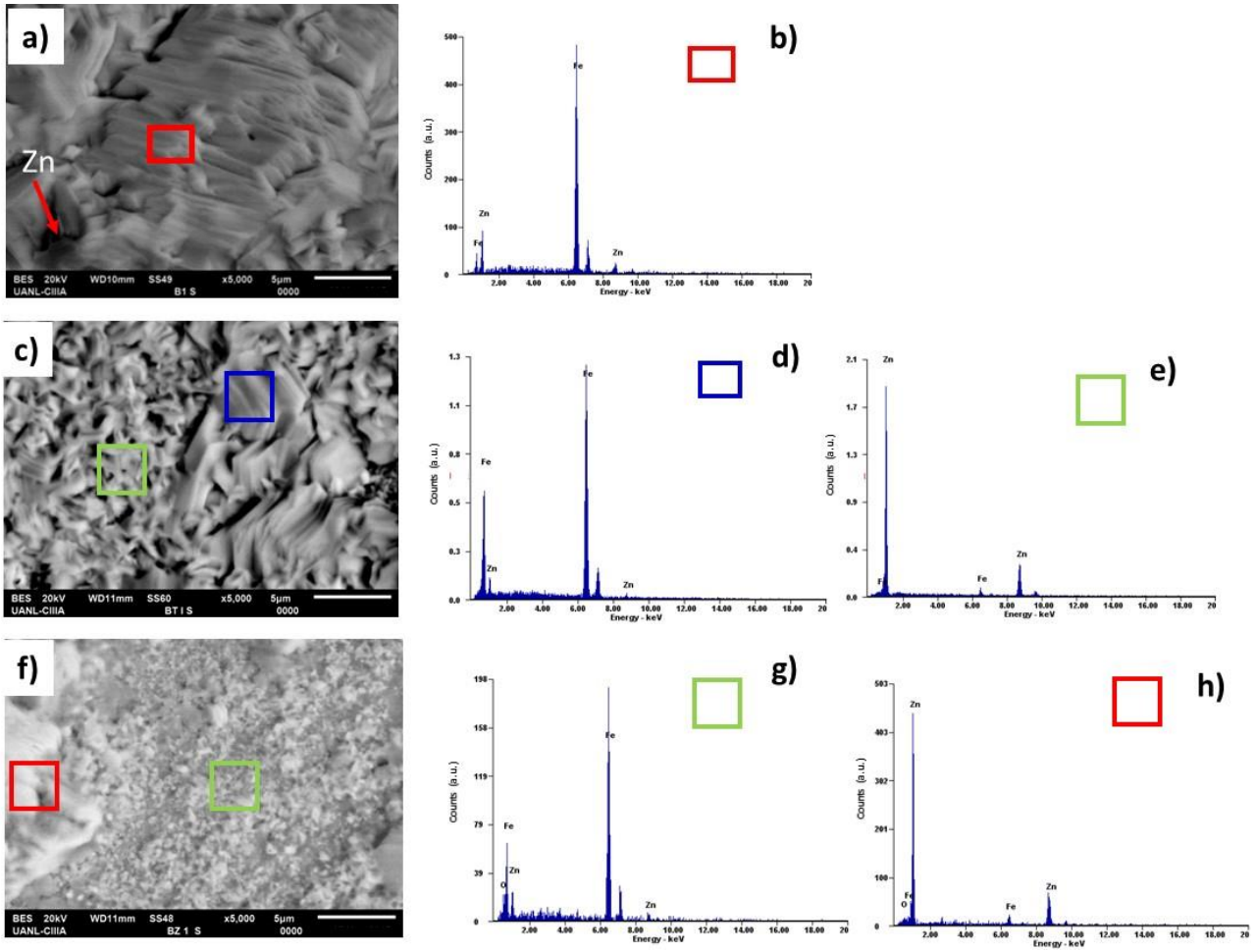

Figure 3. SEM morphology (for 0.05 A/cm^2 current density) for (a) pure zinc coating, (c) Zn-TiO_2 composite coating, and (f) Zn-ZnO composite coating. EDS spectra for (b) pure zinc, (d) and (e) for Zn-TiO_2 composite coating, (g) and (h) for Zn-ZnO composite coating.

Fig. 4 shows the morphology of the pure zinc (Fig. 4(a)) and Zn-TiO_2 (Fig. 4(c)) deposits, revealing non-uniform crystal growth. These coatings present a hexagonal morphology and the specimens with nanoparticles show a smaller grain size. The crystals are homogeneous and randomly size-distributed in the pure zinc and Zn-TiO_2 composite coatings. The Zn-ZnO coating, Fig. 4(e), shows

a homogeneous fibre morphology. In the EDS spectra, Fig. 4(b,d,f), the presence of Zn and a very small Fe signal is observed. During the electroposited process the crystal size was controlled by the formation rate of new nucleation sites or the crystal growth rate. Fine-grained deposits are generally obtained with a faster formation of nucleation sites as a result of heterogeneous nucleation.

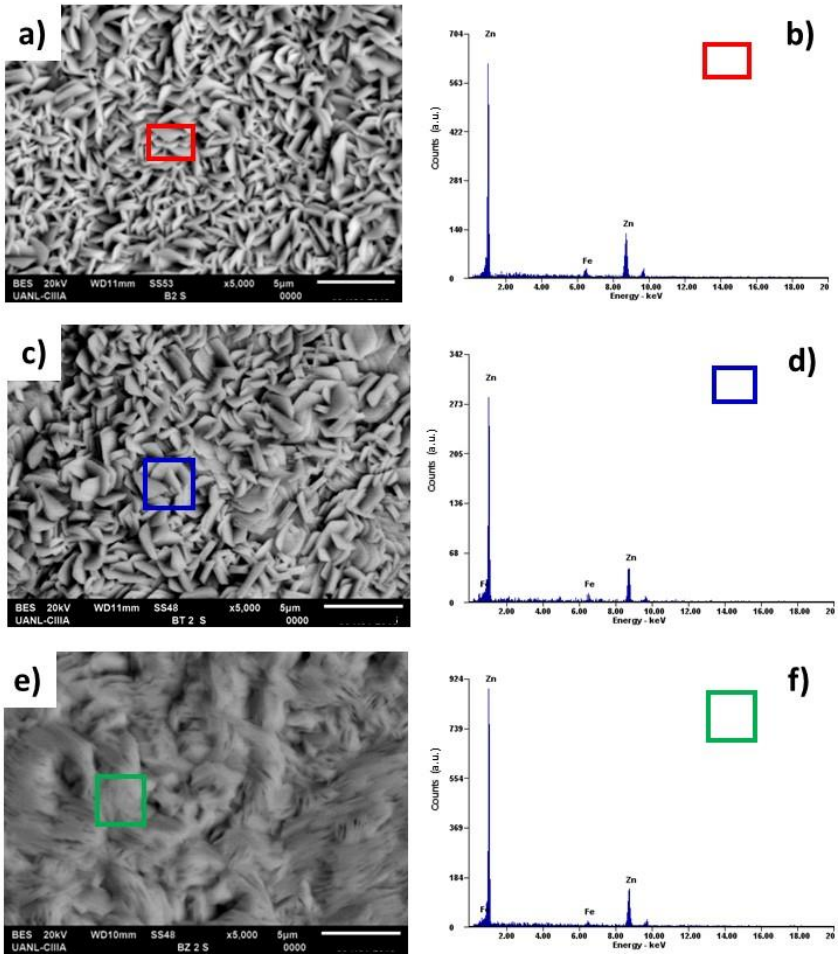

Figure 4. SEM morphology (for 0.10 A/cm^2 current density) for (a) pure zinc coating, (c) Zn-TiO_2 composite coating, and (e) Zn-ZnO composite coating. EDS spectra for (b) pure zinc, (d) for Zn-TiO_2 composite coating, (f) for Zn-ZnO composite coating.

3.3 Potentiodynamic Polarization

The potentiodynamic polarization for pure zinc, Zn-TiO_2 and Zn-ZnO composite coating specimens are shown in Figs. 5 and 6. Coatings were electrodeposited using 0.05 A/cm^2 and 0.10 A/cm^2 current densities, respectively, and immersed in a 3.5% NaCl test solution. The polarization curve shifts to more positive potentials in the case of specimens with Zn-TiO_2 and Zn-ZnO nanoparticles. This potential ennoblement may be produced by compactly electrodeposited zinc layers, presenting very homogenously distributed nanoparticles on zinc grains, without secondary or segregated phases, as shown in Fig. 4. The shift in potential to more positive values is the result of zinc oxide stability formed

in a neutral or slightly alkaline solution. In the cathodic direction this change reduces the hydrogen evolution process and the corrosion rate. Thus, polarization curves show that corrosion rate decreased when different nanoparticles were added during the electroposited process.

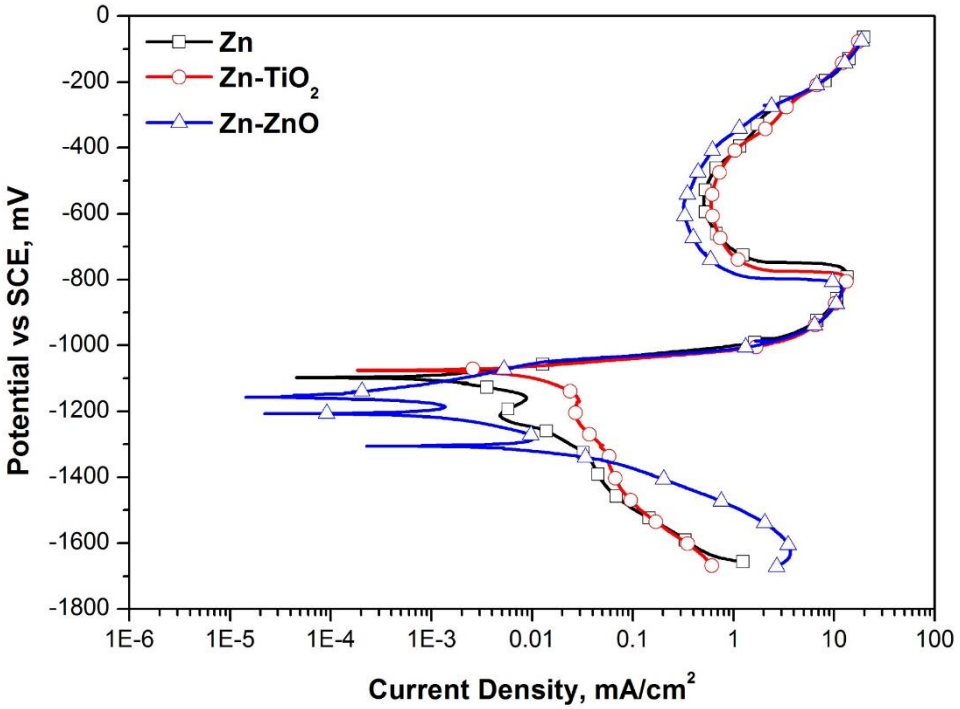

Figure 5. Potentiodynamic polarization curves for pure zinc coating and composite coatings samples Zn-TiO_2 and Zn-ZnO obtained using a current density of 0.05 A/cm^2 and immersed in 3.5% NaCl solution.

The Potentiodynamic polarization present two different crossover potentials for all three electrodeposited specimens, which may be explained as alternate cathodic and anodic behaviour of the system, depending mainly upon the partial current density sign for each process (positive for anodic and negative for cathodic processes). Thus explaining the increase of the total current density for the anodic process, up to 0.01 mA/cm^2, and suddenly after a protective layer formed, the final resulting current density sharply decreases down to 10^{-6} mA/cm^2, The loop at potentials near −1200 mV vs. SCE may be attributed to the protective formation of a ZnO film, i.e. during the oxidation of zinc a release of Zn^{2+} species occurs, thus forming oxides that may be deposited on the metal surface and hinder the subsequent dissolution of the electrodeposited zinc coating.

The anodic process of zinc was completed after a higher current density value was achieved, 20 mA/cm^2, leading to complete dissolution of the electrodeposited coating. Furthermore, the protective layer loss enables the activation and further corrosion of the steel substrate. As observed in the polarization tests (Figs. 5 and 6), the curves presented a loop close to –600 mV vs. SCE, thus corresponding to the redox potential of iron.

It may be pointed out that the influence of the pH value conditions and oxygen content in the test solution play an important role in the corrosion behaviour of electrodeposited iron substrates. Thus the Fe-Zn/electrolyte system presents completely different behaviour depending on the pH and oxygen concentration. Corrosion dissolution of the zinc alloy surface on the steel substrates exposed to chloride-containing solutions varies according to the pH. In the outermost electrodeposited zinc layer, the pH presents a high value.

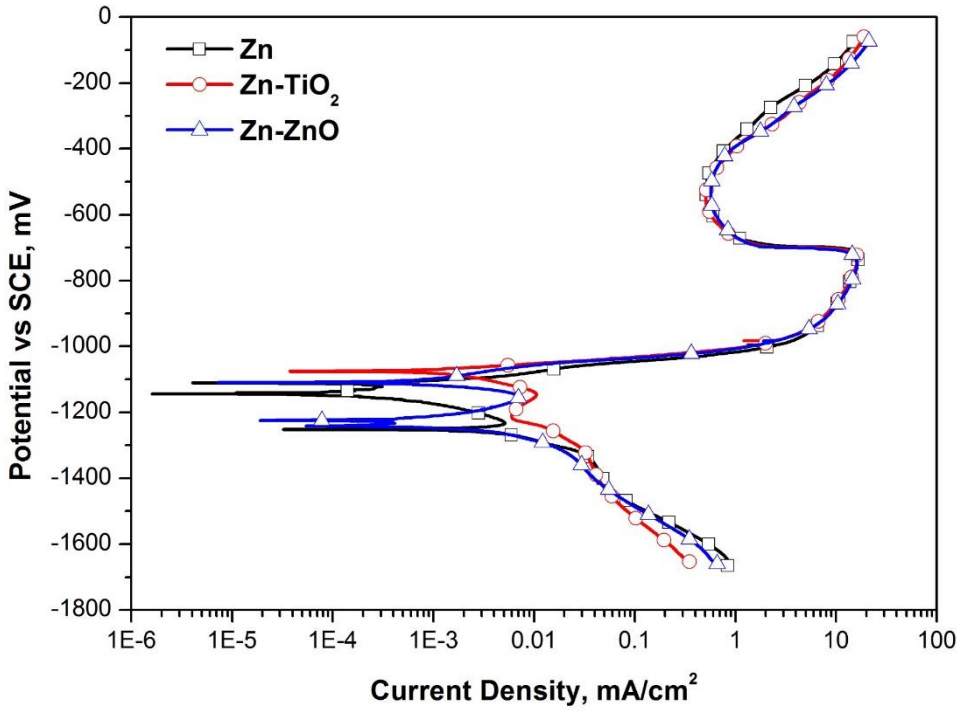

Figure 6. Potentiodynamic polarization for pure zinc coating and Zn-TiO_2 and Zn-ZnO composite coating samples obtained using a current density of 0.10 A/cm^2 and immersed in 3.5% NaCl solution.

The zinc oxidation half-reaction shown in Eq. (1) accounts for the high pH indicated as a result of the anodic zinc dissolution process, where the oxygen reduction half-reaction delivers OH^- ions, Eq. (2). The zinc oxidation overall reaction is presented in Eq. (3). The surface areas in contact with the electrodeposited zinc layer present a low pH value, and this lower pH is promoted by the zinc metal acid hydrolysis according to Eq. (4), thus producing H^+ species:

$$Zn \rightarrow Zn^{2+} + 2e^- \quad (1)$$

$$1/2O_2 + H_2O + 2e^- \rightarrow 2OH^- \quad (2)$$

$$2Zn + O_2 + 2H_2O \rightarrow 2Zn(OH)_2 \quad (3)$$

$$Zn^{2+} + H_2O \rightarrow ZnOH^+ + H^+ \quad (4)$$

On the metal surface where the pH value is low, a high release of Zn^{2+} species takes place. However, there are no Zn^{2+} species in the outermost layer of the zinc electrodeposit, because a high pH applies and thus $Zn(OH)_2$ is found. The corrosion mechanism for zinc electrodeposited coatings on steel substrates is a result of the different concentration distribution of several species such as H^+, OH^- and Zn^{2+}. A non-steady state process governs the overall corrosion mechanism, since zinc acid hydrolysis continuously releases Zn^{2+} and H^+ species, as is shown in Eq. (4). Moreover, chlorides induce anodic dissolution on the zinc surface which occurs as a result of the oxygen reduction, thus leading to the formation of a protective $Zn_5Cl_2(OH)_8{\cdot}H_2O$ compound, as is shown in Eq. (5), and ultimately ZnO will form while high pH conditions apply, see Eq. (6) [19]:

$$5Zn^{2+} + H_2O + 8OH^- + 2Cl^- \rightarrow Zn_5Cl_2(OH)_8{\cdot}H_2O \quad (5)$$

$$Zn^{2+}\ 1/2O_2 + 2e^- \rightarrow ZnO \quad (6)$$

The nanoparticle composite coatings of Zn-TiO_2 and Zn-ZnO (using both 0.05 and 0.10 A/cm^2 current density) are stable in contact with the 3.5% NaCl aggressive medium when compared to the pure zinc coating. Table 1 shows the obtained values from potentiodynamic polarization curves of zinc and composite nano-Zn. Zinc coating corrosion current density (i_{corr}) values were 2.3×10^{-3} mA/cm^2 (electrodeposited using 0.05 A/cm^2) and 1.9×10^{-3} mA/cm^2 (electrodeposited using 0.1 A/cm^2) were lower in terms of i_{corr}. However, i_{corr} values are similar for composite coatings (see Table 1).The effect of TiO_2 and ZnO nanoparticles on corrosion behaviour is to minimize the appearance of defects that act as active sites for corrosion. On the other hand, it may be that the TiO_2 and ZnO nanoparticles are evenly distributed on the surface and behave as a passive layer. Current density will affect the deposition rate, current efficiency the Zn-TiO_2 and Zn-ZnO composite coating [20,21].

Table 1. Obtained electrochemical parameters using potentiodynamic polarization.

Sample	***E_{corr} mV_{SCE}***	***i_{corr} mA/cm^2***	***v_{corr} mm/year***
0.05 A/cm^2			
Zn	*−1102*	*2.3×10^{-3}*	*3.4×10^{-2}*
Zn-TiO_2	*−1071*	*9.0×10^{-3}*	*13.5×10^{-2}*
Zn-ZnO	*−1156*	*0.1×10^{-3}*	*0.7×10^{-2}*
0.1 A/cm^2			
Zn	*−1143*	*1.9×10^{-3}*	*2.8×10^{-2}*
Zn-TiO_2	*−1109*	*1.4×10^{-3}*	*2.1×10^{-2}*
Zn-ZnO	*−1075*	*1.3×10^{-3}*	*1.9×10^{-2}*

3.4 Electrochemical Impedance Spectroscopy

Figs. 7 and 8 present Nyquist plots of pure zinc, Zn-TiO_2 and Zn-ZnO composite coatings deposited using 0.05 and 0.10 A/cm^2 current density, respectively, and immersed in a 3.5% NaCl test solution. These figures also show the fitting data of the EEC model (see Figs. 7 and 8 upper part), which matches well with the experimental data shown as individual points. The agreement of the data and the low χ^2 values corroborate the accuracy of the proposed EEC model. Table 1 depicts the EIS results of the best fitting procedure, where R_{ct} is the charge transfer resistance (inversely proportional to the corrosion rate) and R_s is the solution resistance, which is approximately constant (15.14−18.84 Ω cm^2), see Table 2. The distributed electrical parameter, the constant phase element (*CPE*), is defined by $Z_{CPE} = (Y_p)^{-1}(j\omega)^{-n}$, where Y_p is the admittance, j^2=(□-1), ω is the angular frequency (rad/s), and the dimensionless n (−1<n<1) is the power of the *CPE* [22]. The value of Y_p is of the order of the double-layer capacitance (10−100 μF/cm^2) typical of a charge transfer process [23].

Table 2. Fitting parameters for pure zinc, Zn-TiO_2 and Zn-ZnO samples using EIS data. The electrical equivalent circuit (EEC) is shown in upper part of Figs. 7 and 8.

Specimen	R_s, Ω cm^2	Y_p, μS/cm^2 s^{-n}	n	R_{ct}, Ω cm^2	C, mF/cm^2	R_1, Ω cm^2	Error, %	χ^2
0.05 A/cm^2								
Pure Zn	18.84	17.31	0.88	3448.10	-1.40	-3103.10	<8.40	4x10^{-4}
Zn-TiO_2	15.14	18.30	0.82	390.70	-76.75	-263.22	<6.24	4x10^{-3}
Zn-ZnO	18.82	11.91	0.80	1950.04	-18.66	-906.10	<6.10	3x10^{-3}
0.1 A/cm^2								
Pure Zn	16.31	13.50	0.79	748.12	−5.50	−553.10	<6.22	4x10^{-4}
Zn-TiO_2	15.97	17.72	0.81	1466.02	−30.38	−630.71	<8.80	5x10^{-3}
Zn-ZnO	15.43	18.51	0.85	2107.00	-7.80	-850.13	<4.52	6x10^{-3}

The Nyquist plots (Figs. 7 and 8) show the formation of a well-defined capacitive semicircle at high-medium frequencies, modelled by the *CPE* (the non-ideal capacitance) and the charge transfer (R_{ct}) parameter corresponding to the corrosion process. There is also the presence of an inductive loop at low frequencies, located in the fourth quadrant of the Nyquist plot, which may be attributed to the formation of a protective ZnO/$Zn(OH)_2$ layer as a result of Zn^{2+} species released during the anodic process reacting with OH^- ions, as indicated above. A competitive adsorption-desorption process of passivating-depassivating species [24−26], which was modelled by the CR_1 network with negative values for both C and R_1 parameters (see Table 2), thus gives a positive time constant (τ=CR_1) [27].

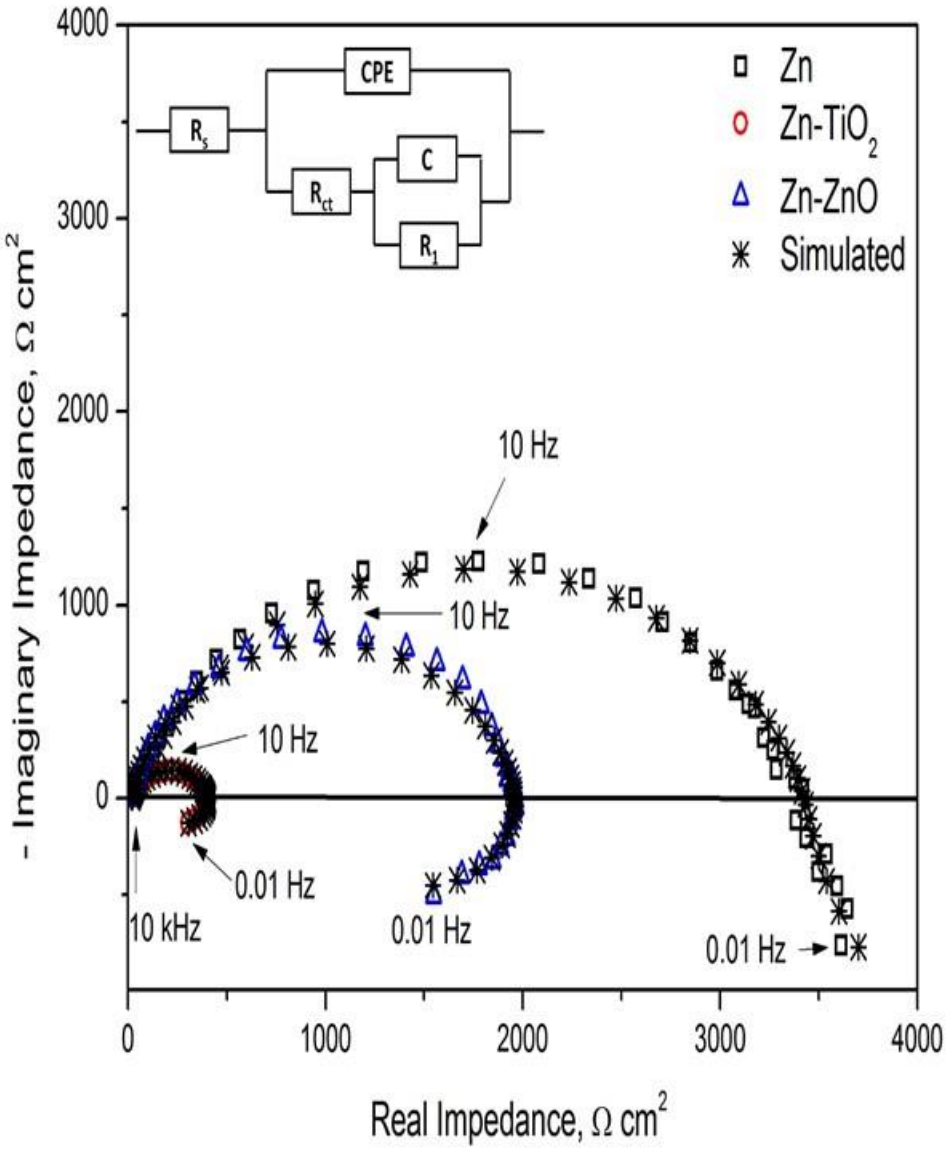

Figure 7. Nyquist plots for pure zinc coating and Zn-TiO_2 and Zn-ZnO composite coating samples obtained using a current density of 0.05 A/cm^2 and immersed in 3.5% NaCl solution. The electrical equivalent circuit (EEC) used is included in the upper part.

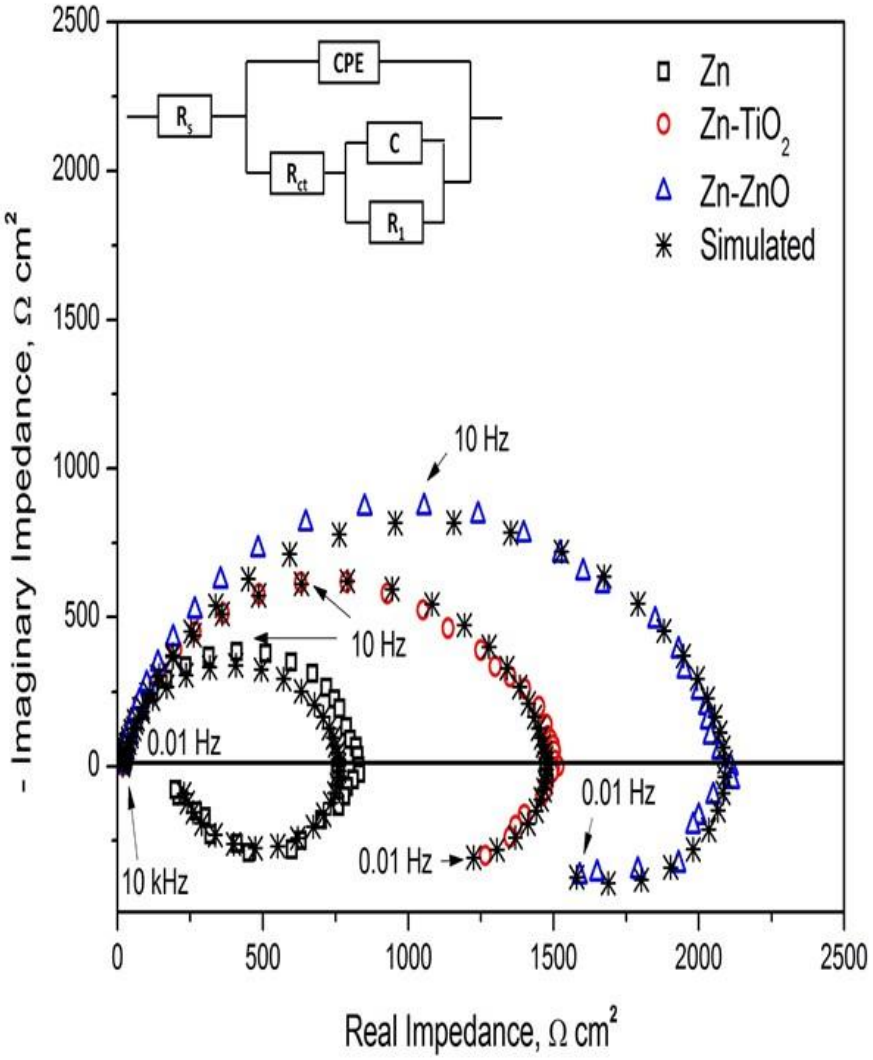

Figure 8. Nyquist plots for pure zinc coating and Zn-TiO_2 and Zn-ZnO composite coating samples obtained using a current density of 0.1 A/cm^2 and immersed in 3.5% NaCl solution. The electrical equivalent circuit (EEC) used is included in the upper part.

The Nyquist plots for a 0.05 A/cm^2 current density (Fig. 7) have a R_{ct} value of 3448.10 Ω cm^2 for the pure zinc coating, 390.70 Ω cm^2 for the Zn-TiO_2 nanoparticle coating, and 1950.04 Ω cm^2 for the Zn-ZnO nanoparticle coating. The lowest R_{ct} value corresponds to the highest corrosion rate, in this case for the Zn-TiO_2 nanoparticle composite coating, see Table 1. These results indicate that the incorporation of TiO_2 nanoparticles does not improve the corrosion resistance, whereas the incorporation of ZnO nanoparticles does.

Impedance results for specimens obtained using a 0.10 A/cm^2 current density (Fig. 8) also show a capacitive loop at high-medium frequencies and an inductive loop below the real axis defined at low frequencies, which may be attributed to adsorption-desorption processes originated by nanoparticles on the electrode surface, similarly to Fig. 7 (for 0.05 A/cm^2 current density). The inductive loop for 0.10

A/cm^2 (see Fig. 8) is better defined than for specimens obtained using a 0.05 A/cm^2 current density (see Fig. 7). This different behaviour may be attributed to the fact that the microstructure of the coating is more compact and homogeneous. Nevertheless, the coating generated with pure zinc has a R_{ct} value of 748.12 Ω cm^2 lower than the R_{ct} for pure zinc (3448.10 Ω cm^2) using 0.05 A/cm^2 current density, see Table 1. The R_{ct} value of 748.12−2107.00 Ω cm^2 for pure zinc, Zn-TiO_2 and Zn-ZnO nanoparticles indicates a higher corrosion resistance than the coatings obtained using a 0.05 A/cm^2 current density, with the exception of the pure zinc coating, as indicated above. The incorporation of TiO_2 and ZnO nanoparticles improves the corrosion resistance of the zinc coating. These results agree well with polarization results (Fig. 5 and 6).

The corrosion behaviour of the coatings with incorporating nanoparticles may be due to the fact that the addition of these components promotes a uniform coating, inhibits the evolution of hydrogen at the cathode, and achieves greater refinement of the grain size of the coating. Some authors have suggested several hypotheses to explain the effects of nanoparticles on corrosion resistance, such as an increase in the cathode surface area due to the adsorbed particles, which change the texture promoted by the nanoparticles and component migration [28,29], and the turbulent flow caused by the nanoparticles [30]. Finally, electrochemical tests revealed that zinc composite coatings containing ZnO nanoparticles obtained using a 0.10 A/cm^2 current density presented higher corrosion resistance than either the pure zinc coating or the composite coatings containing TiO_2 nanoparticles. An increase in current density leads to a more rapid deposition of the metallic matrix, depends on the nano particles characteristic (type, size and shape) [31].

4. CONCLUSIONS

• Coatings containing Zn-nanoparticles and with a thickness of less than 2.5 μm were successfully electrodeposited on steel sheets from a zinc electrolyte.

• The nanoparticle-containing electrodeposited coatings of Zn-TiO_2 and Zn-ZnO, obtained using 0.10 A/cm^2 of current density, showed good corrosion resistance when evaluated using potentiodynamic and impedance electrochemical techniques.

• The electrodeposited coated steel substrate presented a corrosion process around –1.2 V vs. SCE, thus showing a huge gap compared to the anodic dissolution found for an iron substrate (approximately at –0.6 V vs. SCE), thus indicating that zinc and Zn-TiO_2 or Zn-ZnO composite coatings containing nanoparticles (TiO_2 and ZnO) cathodically protected steel by acting as a sacrificial anode.

• The corrosion current density was lower in the composite coating electrodeposited using a 0.10 A/cm^2 current density with additions of ZnO nanoparticles.

ACKNOWLEDGEMENTS

The authors would like to acknowledge the work group UANL-CA-316, and P.O. Samaniego G. D.M. Bastidas gratefully acknowledges funding from The University of Akron. Paper in memoriam of Dr. Alberto Martinez-Villafañe (†).

References

1. J.A. Switzer, G. Hodes, *Mater. Res. Bull.*, 35 (2016) 743.
2. B.M. Praveen, T.V. Venkatesha, *Int. J. Electrochem. Sci.*, 4 (2009) 258.
3. J.M. Li, C. Cai, L.X. Song, J.F. Li, Z. Zhang, M.Z. Xue, Y.G. Liu, *Trans. Nonferrous Met. Soc. China*, 23 (2013) 2300.
4. C.T.J. Low, R.G.A. Wills, F.C. Walsh, *Surf. Coat. Technol.*, 201 (2006) 371.
5. M. Chandran, G.K. Ramesh-Bapu, *Acta Chim. Pharm. Indica*, 3 (2013) 219.
6. B. Xue, Y. Liang, L. Donglai, N. Eryong, S. Congli, F. Huanhuan, X. Jingjing, J. Yong, J. Zhifeng, S. Xiaosong, *Appl. Surf. Sci.*, 257 (2011) 10317.
7. O. Hammami, L. Dhouibi, E. Triki, *Surf. Coat. Techno.l*, 203 (2009) 2863.
8. V. Thangaraj, A. Chitharanjan-Hegde, *Indian J. Chem. Technol.*, 14 (2007) 246.
9. M.K. Punith-Kumar, T.V. Venkatesha, *J. Chem. Pharm. Res.*, 5 (2013) 253.
10. A. Grosjean, M. Rezrazi, J. Takadoum, P. Bercot, *Surf. Coat. Technol.*, 137 (2001) 92.
11. P.A. Gay, P. Bercot, J. Pagetti, *Surf. Coat. Techno.l*, 140 (2001) 147.
12. J. Wang, C. Cai, S.L. Ma, Z. Zhang, J.Q. Zhang, *Chinese J. Chem. Phys.*, 23 (2010) 347.
13. T. Tsuru, S. Kobayashi, T. Akiyama, H. Fukushima, S.K. Gogia, R. Kammel, *J. Appl. Electrochem.*, 27 (1997) 209.
14. T. Frade, J. Melo, A. Gomes, *Surf. Coat. Technol.*, 206 (2012) 3459.
15. J.S. Wellings, N.B. Chaure, S.N. Heavens, I.M. Dharmadasa, *Thin Solid Films*, 516 (2008) 3893.
16. T. Frade, V. Bouzon, A. Gomes, M. Da Silva Pereira, *Surf. Coat. Technol.*. 204 (2010) 3592.
17. ASTM G5-11, Standard reference test method for making potentiostatic and potentiodynamic anodic polarization measurements, (2011), West Conshohocken, PA. USA.
18. ASTM G106-15, Standard practice for verification of algorithm and equipment for electrochemical impedance measurements, (2015), West Conshohocken, PA. USA.
19. E. Tada, S. Satoh, H. Kaneko, *Electrochim. Acta*, 49 (2004) 2279
20. L. Ma, X. Xi, Z. Nie, T. Dong, Y. Mao, *Int. J. Electrochem. Sc.i*, 12 (2017) 1034.
21. F. D. Ruiz-Ocampo, J. M. Zapien-Rodríguez, O. Burgara-Montero, E. A. Escoto-Sotelo, F. A. Núñez-Pérez, J. C. Ballesteros-Pacheco, *Int. J. Electrochem. Sci.*, 12 (2017) 4898.
22. A.K. Manohar, O. Bretschger, K.H. Nealson, F. Mansfeld, *Bioelectrochemistry*, 72 (2008) 149.
23. D.A. Miranda, S.A. Jaimes, J.M. Bastidas, *J. Solid. State Electrochem.*, 18 (2014) 389.
24. M. Bojinov, G. Fabricius, P. Kinnunen, T. Laitinen, K. Mäkelä, T. Saario, G. Sundholm, *Electrochim. Acta*, 45 (2000) 2029.
25. U. Rammelt, G. Reinhard, K. Rammelt, *J. Electroanal. Chem.*, 180 (1984) 327.
26. J.L. Polo, C.L. Torres, E. Cano, J.M. Bastidas, *Rev. Metal*, 35 (1999) 368.
27. J.M. Bastidas, J.L. Polo, C.L. Torres, E. Cano, *Corros. Sc.i*, 43 (2001) 269.
28. L. Benea, P.L. Bonora, A. Borello, S. Martelli, F. Wenger, P. Pouthiaux, J. Galland, *J. Electrochem. Soc.*, 148 (2001) C461.
29. R.P. Socha, P. Nowak, K. Laajalehto, J. Väyrynen, *Colloid. Surface A Phy. Eng. Aspect*, 235 (2004) 45.
30. X. Xia, I. Zhitomirsky, J.R. Mcdermid, *J. Mater. Process. Technol*, 209 (2009) 2632.
31. G. Roventi, G. Giuliani, M. Pisani, T. Bellezze, *Int. J. Electrochem. Sci.*, 12 (2017) 663.